

**Angular velocity along mid-ocean ridges,
and the unexpected variation
in the length of transform faults**

Ryley M. Collins and Vincent S. Cronin, Baylor University, Waco, TX 78793, Ryley_Collins@baylor.edu and Vince_Cronin@baylor.edu

Abstract

Many geoscientists assume that ridge-ridge transform faults along mid-ocean ridges have a constant geometry over finite time intervals until or unless some plate-reorganization event occurs. This assumption is based on the first-generation plate-kinematic model in which [1] transform faults were assumed to be concentric around an Euler pole that is fixed to the two plates over finite time intervals and, hence, [2] no convergence or divergence occurs along transform faults and [3] oceanic fracture zones follow small circles concentric to the Euler pole except where perturbed by plate reorganization (e.g., Morgan, 1968; McKenzie and Parker, 1967). These postulates of first-generation plate kinematics were disproven for finite displacements in the early 1970s on purely geometric-kinematic grounds (e.g., Cox, 1973), so plates must generally move in a non-circular finite trajectory relative to each other and the shape, length, and position of transform faults is likely to vary continuously over finite time intervals.

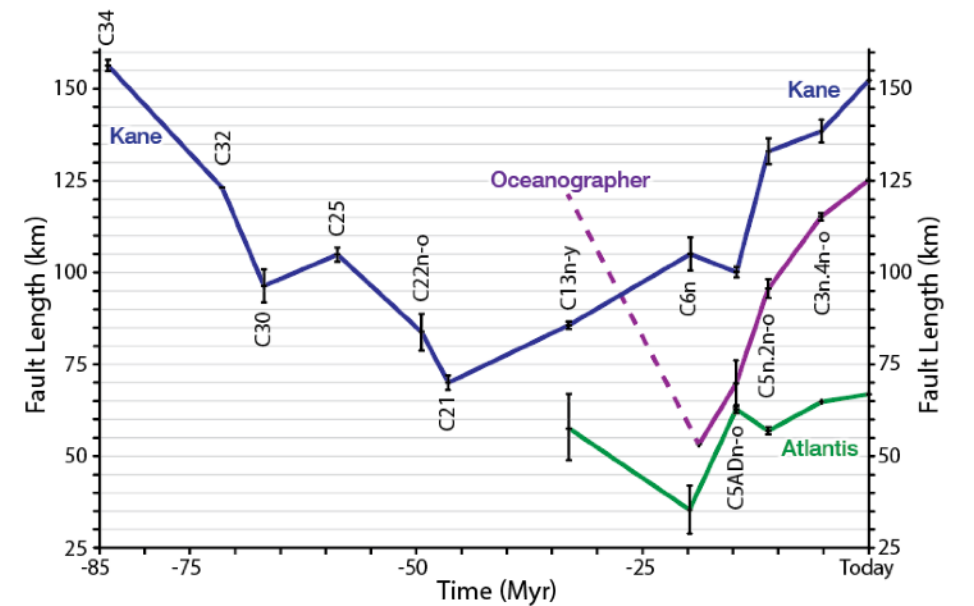
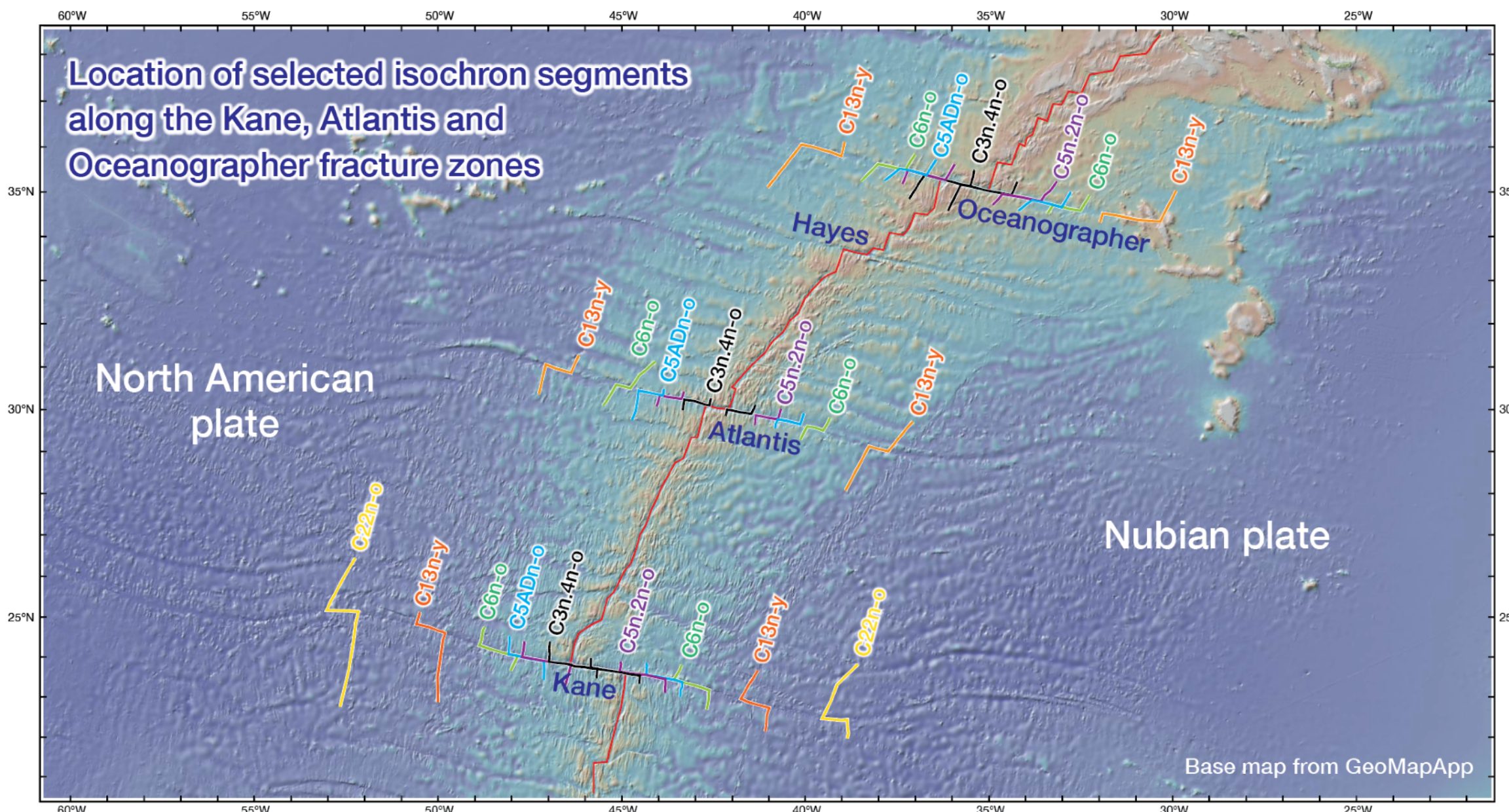
The traces of isochrons defined by marine magnetic anomalies are deflected as they cross oceanic fracture zones. The distance that a given isochron is deflected provides a measure of the approximate length of the transform fault associated with the fracture zone at that time. We used the best published data for the location of isochrons defined by marine magnetic anomalies (www.soest.hawaii.edu/PT/GSFML/) to measure the variation in length of several transform faults during the Cenozoic, including some of the major transforms in the North Atlantic: Kane, Atlantis, Hayes and Oceanographer. The length of R-R transform faults examined in this study seems to have changed continuously over that time interval. For example, the Kane transform fault has lengthened from ~84 km at ~50 Ma, ~106 km at ~20 Ma, and ~133 km at ~11 Ma to its current length of ~153 km. A similar progression was noted for other transforms between the North American and Nubian (west African) plates. Reasons might include the generally non-circular finite relative motion of plates and the instantaneous instability of mid-ocean ridges (Cronin, 1994).

References and other relevant information are accessible via CroninProjects.org/Tectonics-AGU2018/.



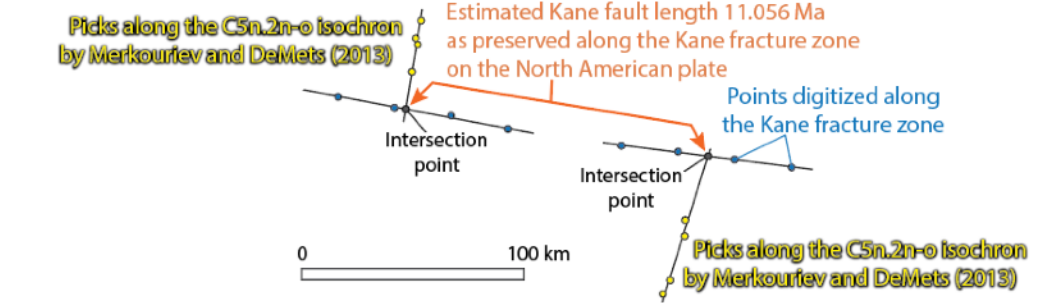
The data used in this analysis were acquired from the *Global Seafloor Fabric and Magnetic Lineation Data Base Project* (PIs Paul Wessel and Dietmar Müller, <http://www.soest.hawaii.edu/PT/GSFML/>). We are grateful for their work in compiling marine magnetic anomaly data and in posting them in a consistent manner on an accessible web portal.

For the north Atlantic ridge between the North American and Nubian (west African) plates, we used isochron data from Merkuriev and DeMets (2013) and Klitgord and Schouten (1986) accessed via <http://www.soest.hawaii.edu/PT/GSFML/ML/index.html>. We ultimately chose to focus on the Kane, Atlantis, and Oceanographer systems and to omit the Hayes system from the present analysis. The initial reason for omitting Hayes is that magnetic data for that system are currently insufficient. The modern Hayes transform fault seems to have lengthened within the past few million years at the expense of a fault that was once located about 0.7° south, whose fracture zone is quite pronounced in older oceanic crust. This apparent reorganization in ridge geometry, along with the relative paucity of magnetic data, makes the Hayes system a poor choice for study in this analysis, but a very good target for further data collection.



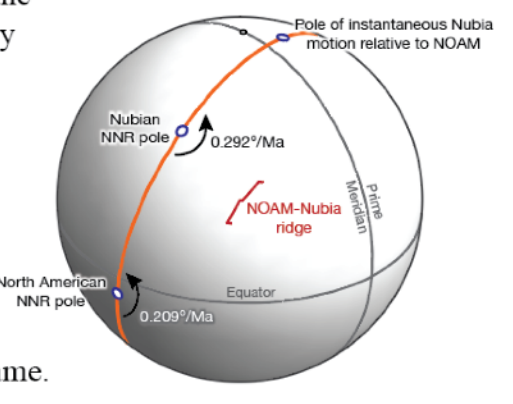
The variation in transform-fault length along the North American-Nubian plate boundary, mid-Atlantic ridge, is shown above.

The fault length was estimated using offset marine-magnetic anomalies along the two oceanic fracture zones (FZ) generated by the transform fault. The point of intersection between the FZ and the anomaly was determined by projecting best-fit great circles for four points along the FZ and (usually) four points along the anomaly near the FZ.



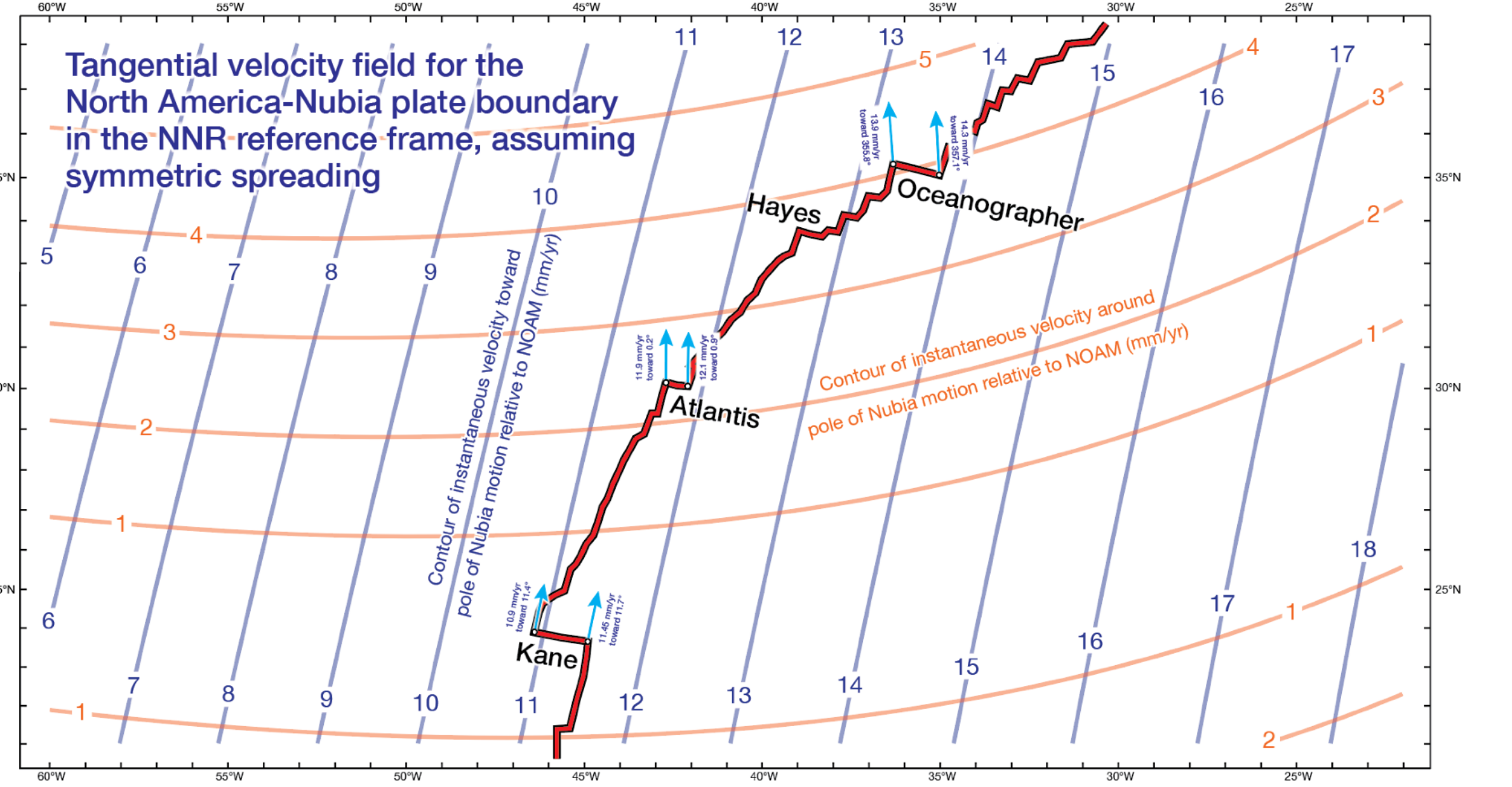
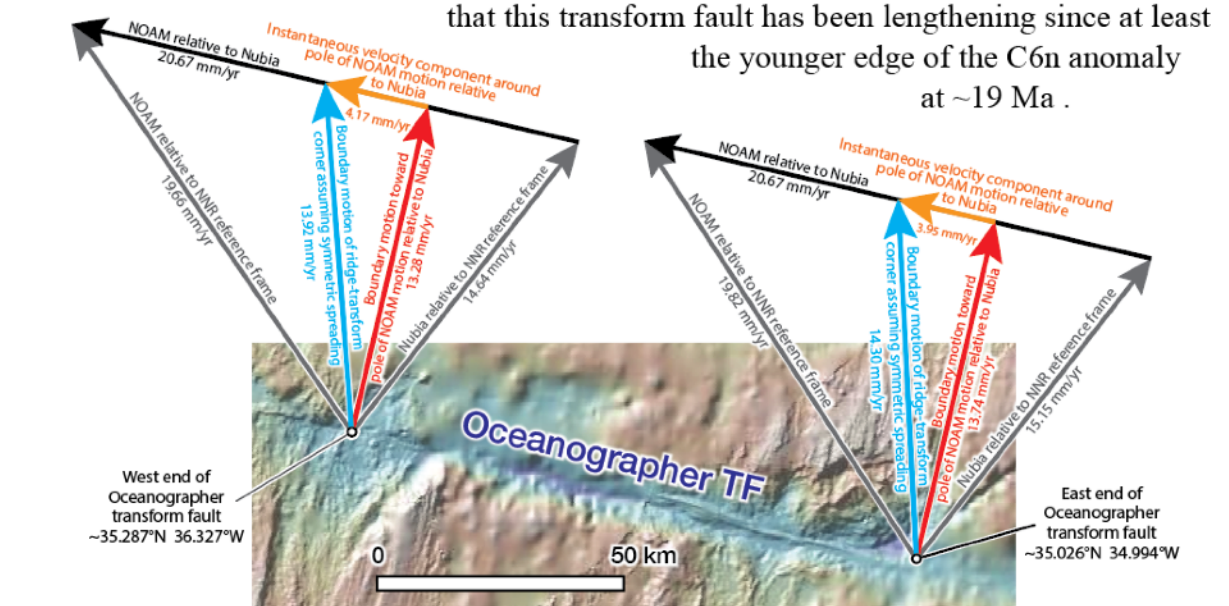
We noted that the estimated fault length for a given isochron is commonly different on the Nubian plate than on the North American plate.

Reasons for the change in R-R transform fault length probably include the generally non-circular finite relative motion of plates and the consequent evolution of transform-fault geometry (Cronin, 1991) and ridge-boundary shape (Cronin, 1994).



The instantaneous plate-motion data used in this study are from DeMets et al. (2010) and Argus et al. (2011). The spatial relationships of the instantaneous-motion poles and the ridge boundary are shown at right. The ridge moves generally north relative to the NNR reference frame.

The instantaneous velocities at the ends of the Oceanographer transform fault, for example, show that the fault moves generally north relative to the NNR reference frame. Assuming symmetric spreading, the differential motion of the two ends of the fault indicate that it should lengthen over time. Offset isochrons across the Oceanographer fracture zones show that this transform fault has been lengthening since at least the younger edge of the C6n anomaly at ~19 Ma.



As the boundary moves in the NNR reference frame (Argus et al., 2011) over finite time intervals, the instantaneous velocity of each point along the boundary changes.

60°W 55°W 50°W 45°W 40°W 35°W 30°W 25°W

Location of selected isochron segments along the Kane, Atlantis and Oceanographer fracture zones

North American plate

Nubian plate

Hayes

Oceanographer

Atlantis

Kane

C13n-y

C6n-o

C5ADn-o

C3n.4n-o

C5n.2n-o

C6n-o

C13n-y

C13n-y

C6n-o

C5ADn-o

C3n.4n-o

C5n.2n-o

C6n-o

C13n-y

C22n-o

C13n-y

C6n-o

C5ADn-o

C3n.4n-o

C5n.2n-o

C6n-o

C13n-y

C22n-o

C13n-y

C6n-o

C5ADn-o

C3n.4n-o

C5n.2n-o

C6n-o

C13n-y

C13n-y

C6n-o

C5ADn-o

C3n.4n-o

C5n.2n-o

C6n-o

C13n-y

C22n-o

C13n-y

C6n-o

C5ADn-o

C3n.4n-o

C5n.2n-o

C6n-o

C13n-y

C22n-o

C13n-y

C6n-o

C5ADn-o

C3n.4n-o

C5n.2n-o

C6n-o

C13n-y

C13n-y

C6n-o

C5ADn-o

C3n.4n-o

C5n.2n-o

C6n-o

C13n-y

C22n-o

C13n-y

C6n-o

C5ADn-o

C3n.4n-o

C5n.2n-o

C6n-o

C13n-y

C22n-o

C13n-y

C6n-o

C5ADn-o

C3n.4n-o

C5n.2n-o

C6n-o

C13n-y

C13n-y

C6n-o

C5ADn-o

C3n.4n-o

C5n.2n-o

C6n-o

C13n-y

C22n-o

C13n-y

C6n-o

C5ADn-o

C3n.4n-o

C5n.2n-o

C6n-o

C13n-y

C22n-o

C13n-y

C6n-o

C5ADn-o

C3n.4n-o

C5n.2n-o

C6n-o

C13n-y

C13n-y

C6n-o

C5ADn-o

C3n.4n-o

C5n.2n-o

C6n-o

C13n-y

C22n-o

C13n-y

C6n-o

C5ADn-o

C3n.4n-o

C5n.2n-o

C6n-o

C13n-y

C22n-o

C13n-y

C6n-o

C5ADn-o

C3n.4n-o

C5n.2n-o

C6n-o

C13n-y

C13n-y

C6n-o

C5ADn-o

C3n.4n-o

C5n.2n-o

C6n-o

C13n-y

C22n-o

C13n-y

C6n-o

C5ADn-o

C3n.4n-o

C5n.2n-o

C6n-o

C13n-y

C22n-o

C13n-y

C6n-o

C5ADn-o

C3n.4n-o

C5n.2n-o

C6n-o

C13n-y

C13n-y

C6n-o

C5ADn-o

C3n.4n-o

C5n.2n-o

C6n-o

C13n-y

C22n-o

C13n-y

C6n-o

C5ADn-o

C3n.4n-o

C5n.2n-o

C6n-o

C13n-y

C22n-o

C13n-y

C6n-o

C5ADn-o

C3n.4n-o

C5n.2n-o

C6n-o

C13n-y

C13n-y

C6n-o

C5ADn-o

C3n.4n-o

C5n.2n-o

C6n-o

C13n-y

C22n-o

C13n-y

C6n-o

C5ADn-o

C3n.4n-o

C5n.2n-o

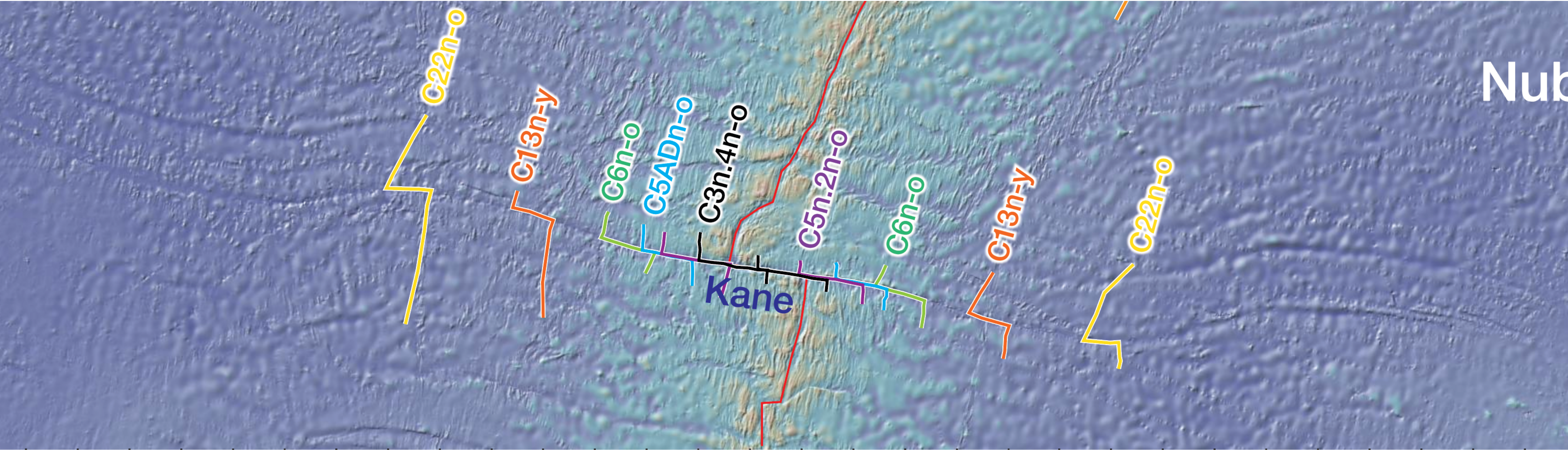
C6n-o

C13n-y

C22n-o

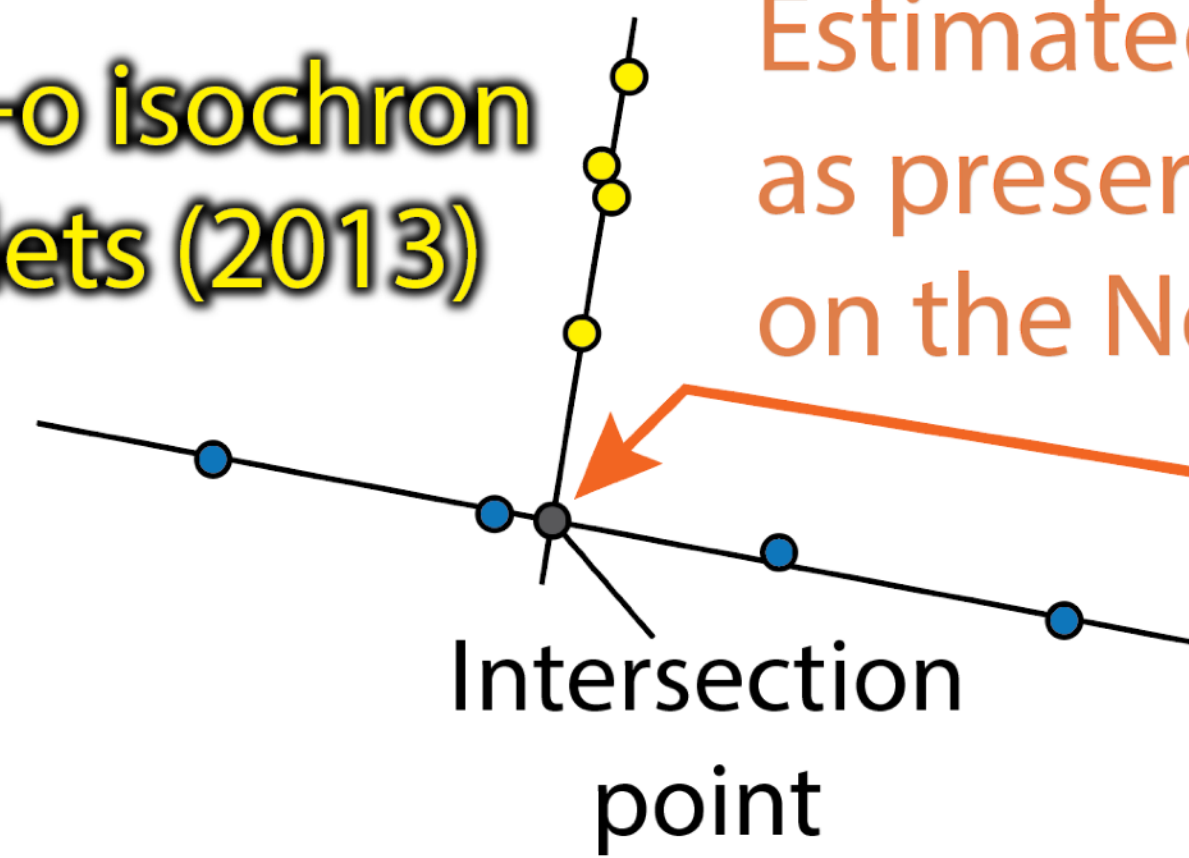
Base map from GeoMapApp

60°W 55°W 50°W 45°W 40°W 35°W 30°W 25°W



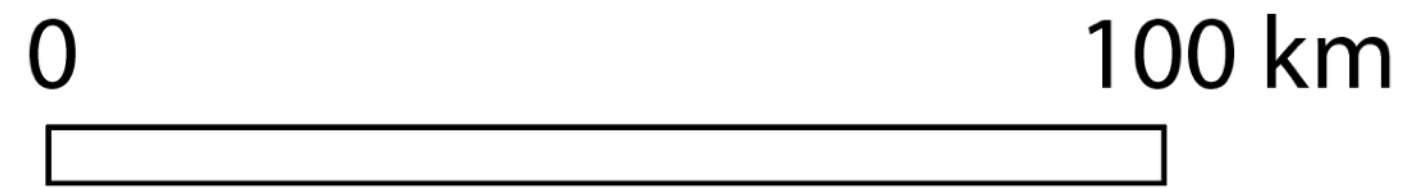
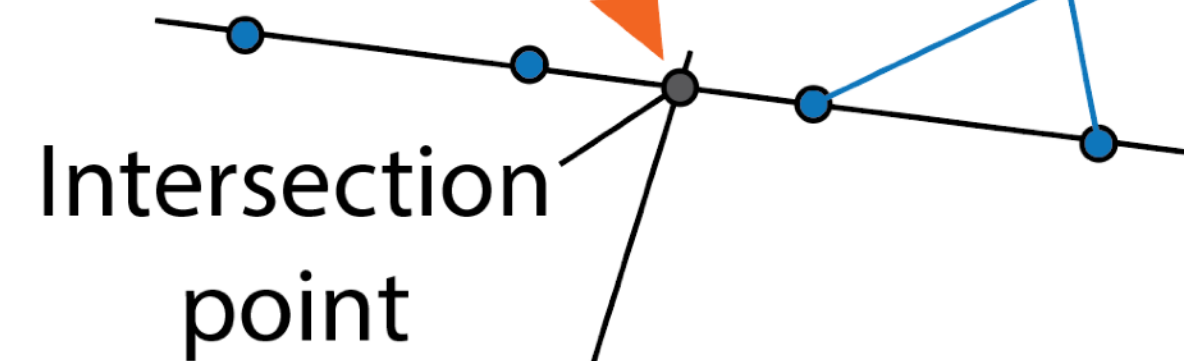
Nub

Picks along the C5n.2n-o isochron
by Merkouriev and DeMets (2013)



Estimated Kane fault length 11.056 Ma
as preserved along the Kane fracture zone
on the North American plate

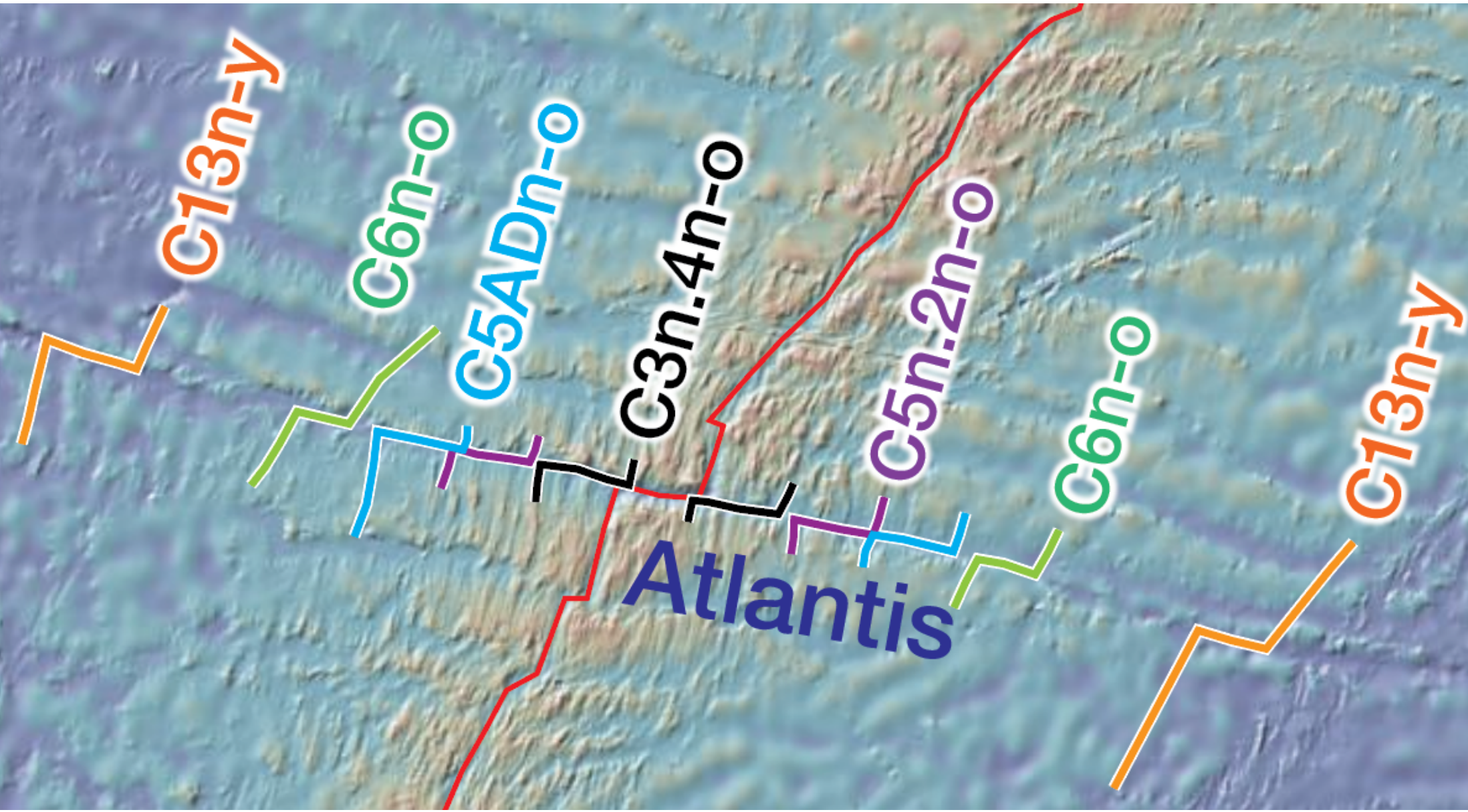
Points digitized along
the Kane fracture zone



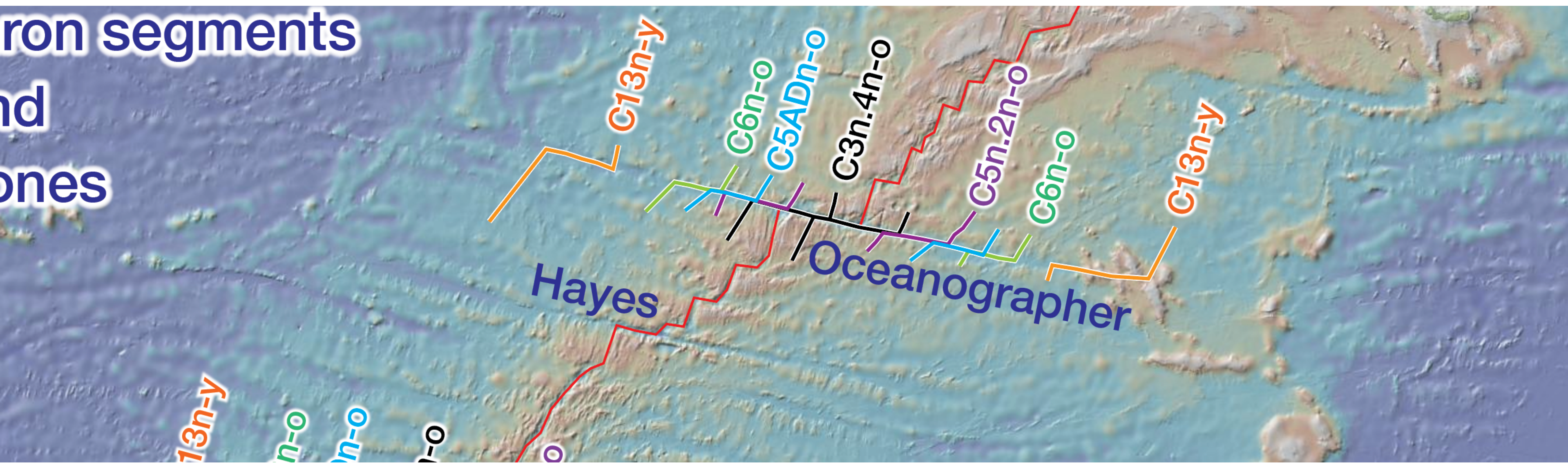
Picks along the C5n.2n-o isochron
by Merkouriev and DeMets (2013)

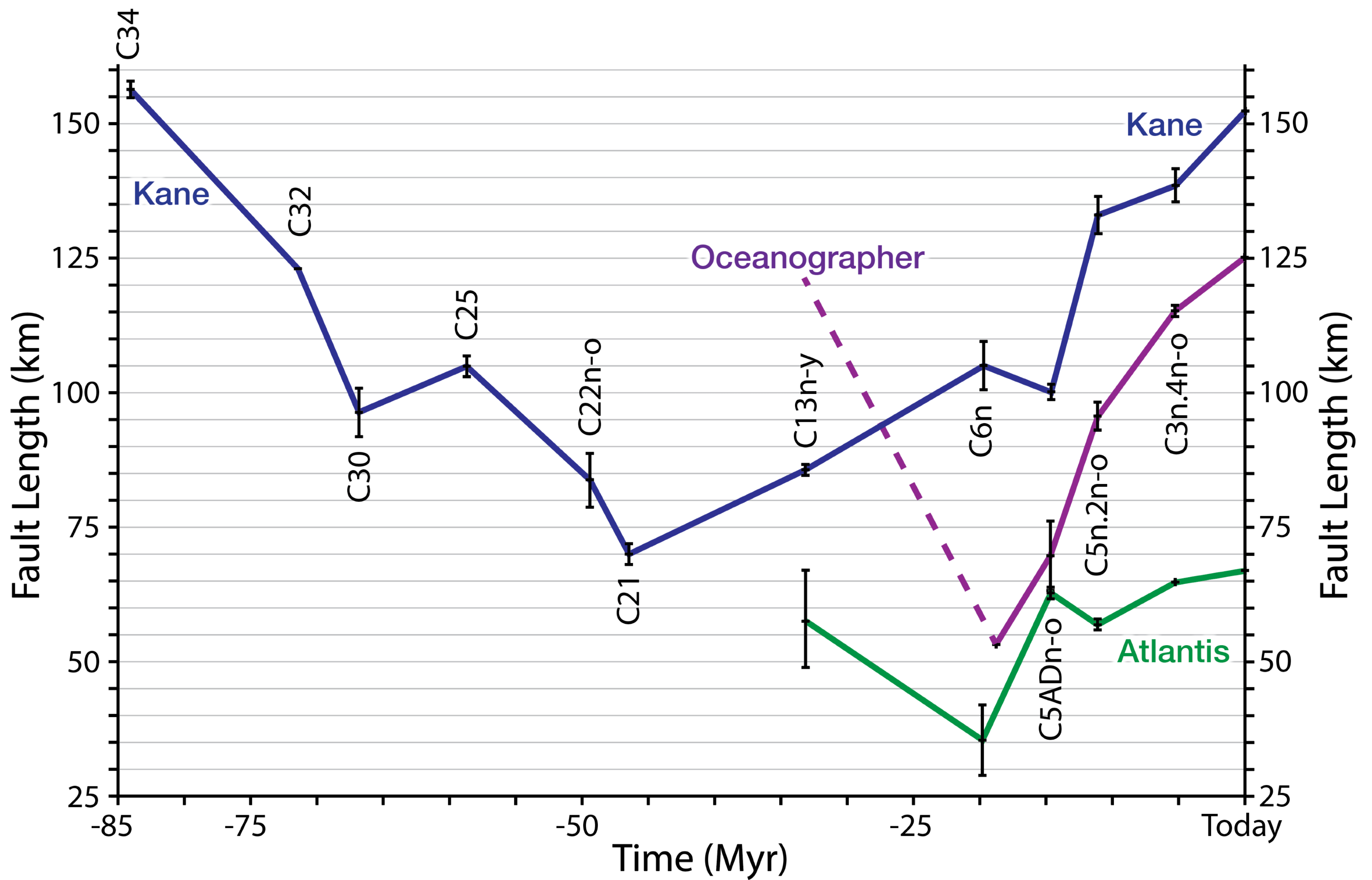


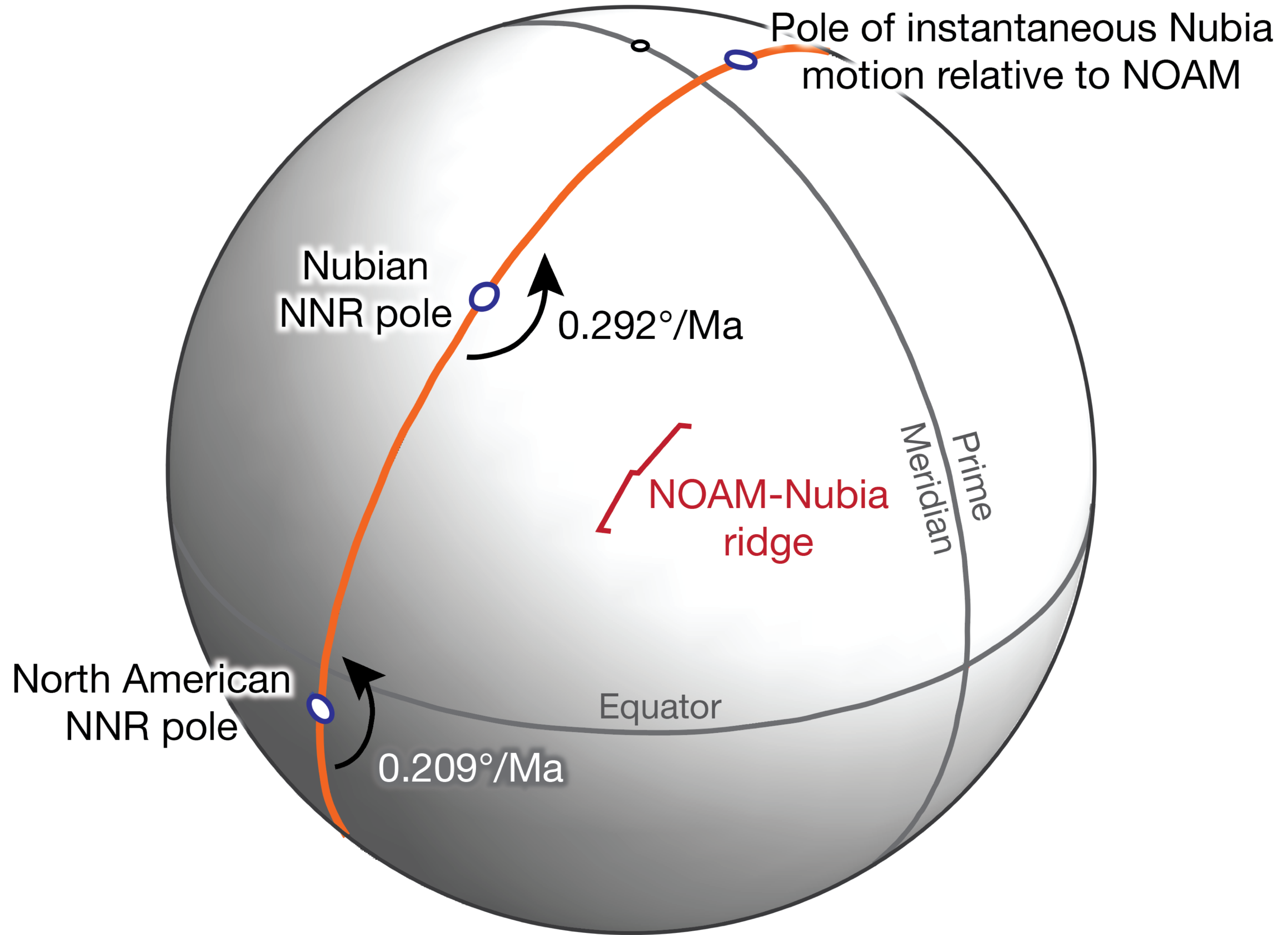
American
ate



Iron segments
and
zones







60°W 55°W 50°W 45°W 40°W 35°W 30°W 25°W

Location of selected isochron segments along the Kane, Atlantis and Oceanographer fracture zones

North American plate

Nubian plate

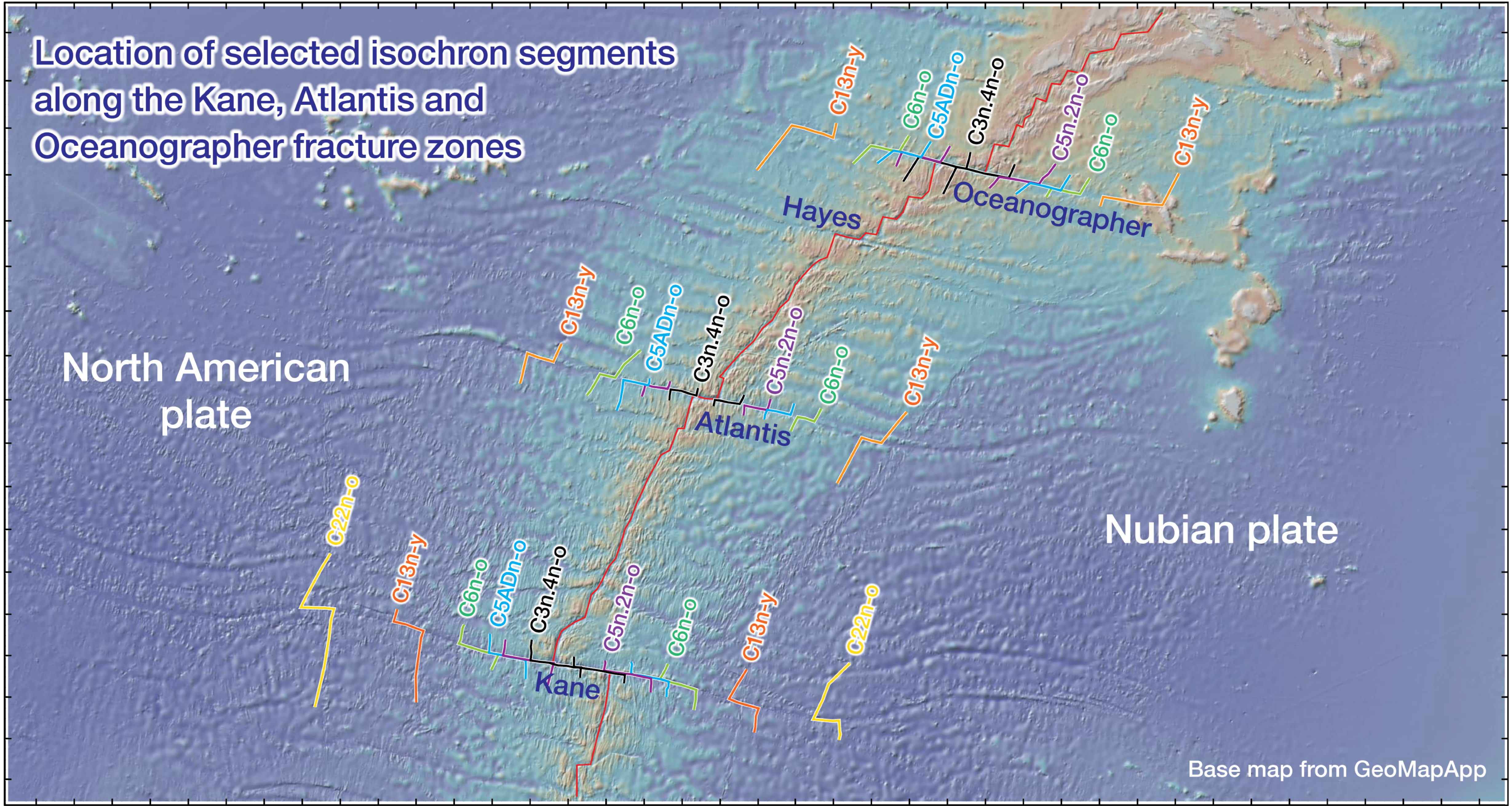
Hayes

Oceanographer

Atlantis

Kane

Base map from GeoMapApp





ELSEVIER

Tectonophysics 230 (1994) 151–159

TECTONOPHYSICS

Instantaneous velocity of mid-ocean ridges

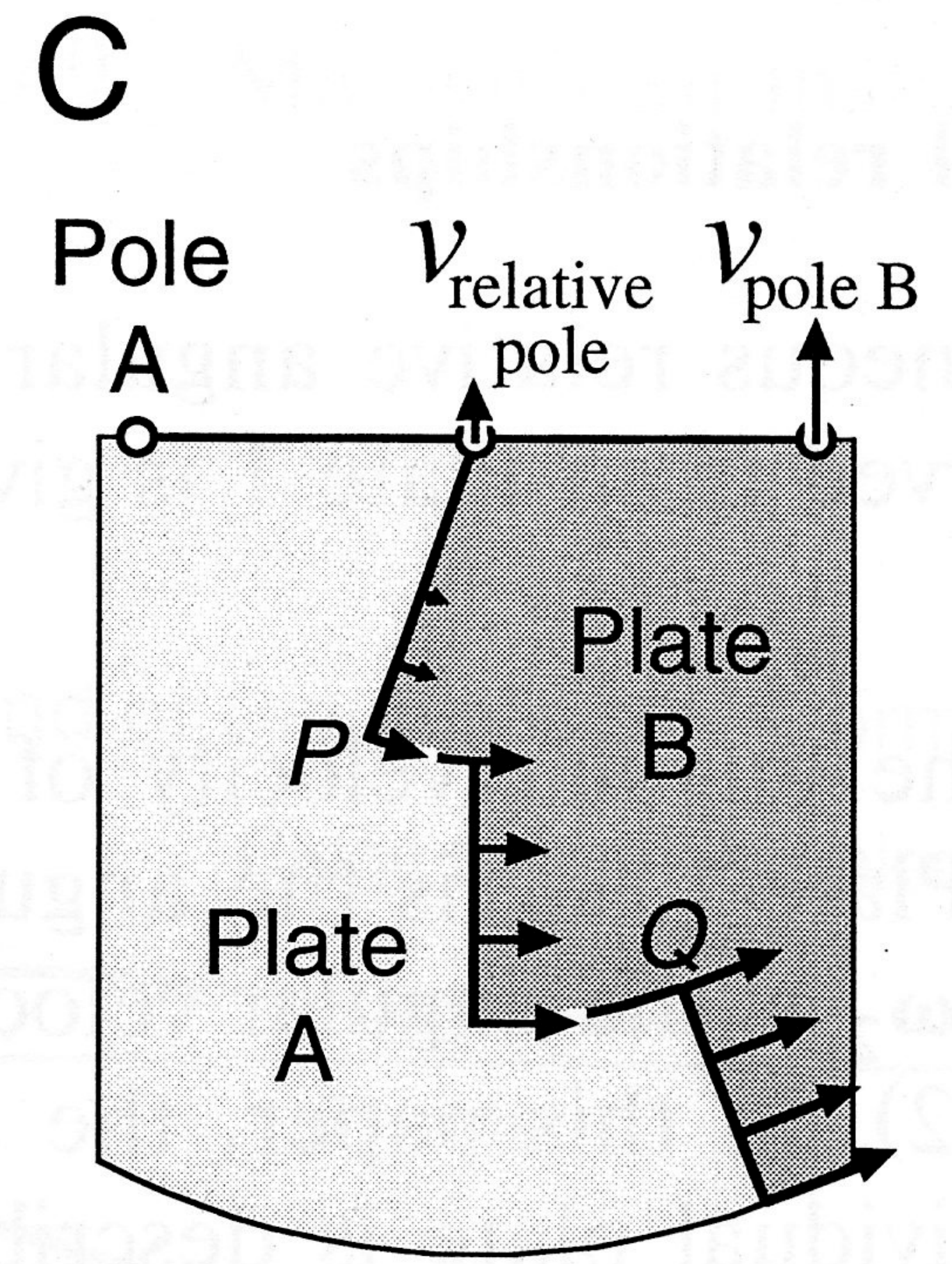
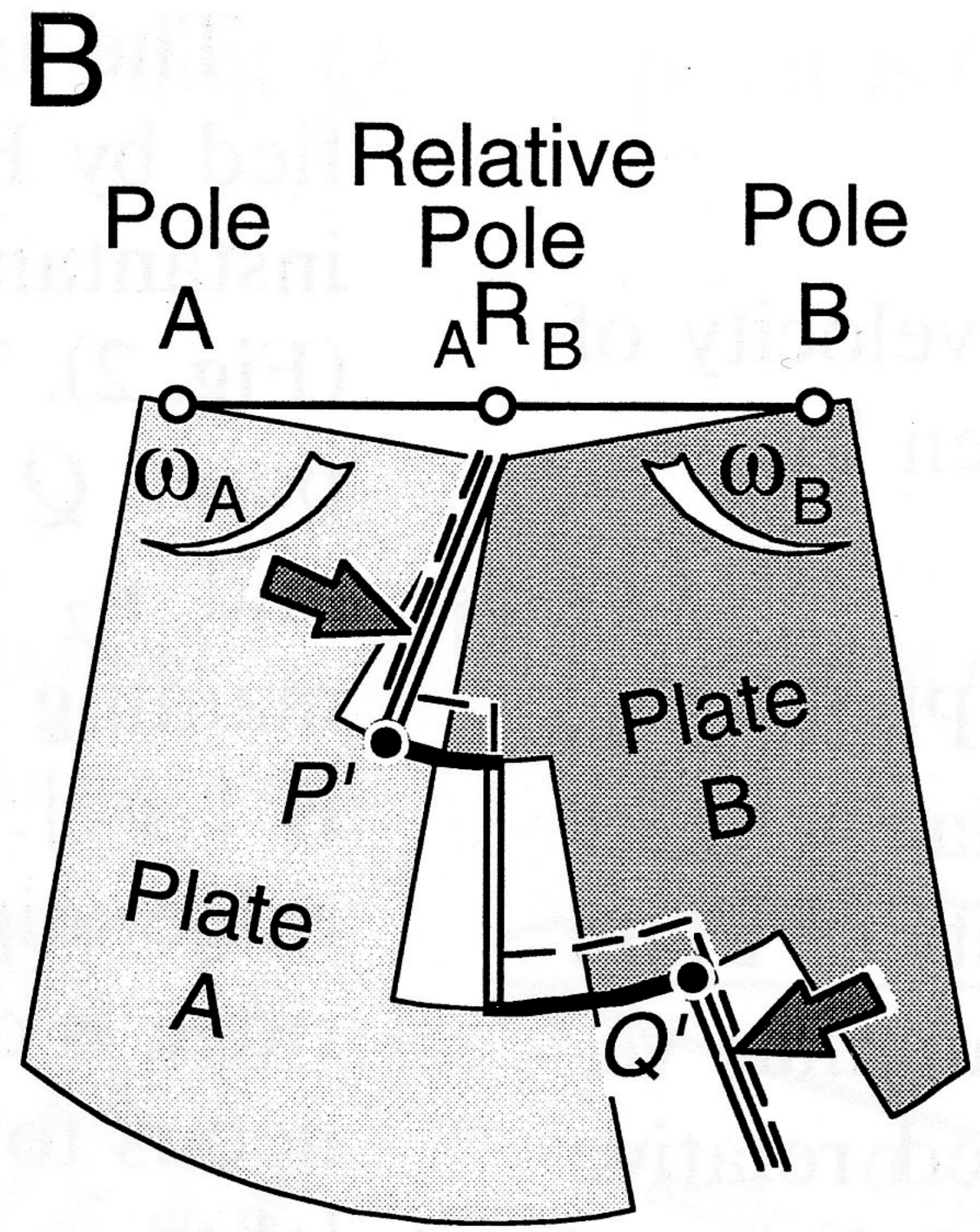
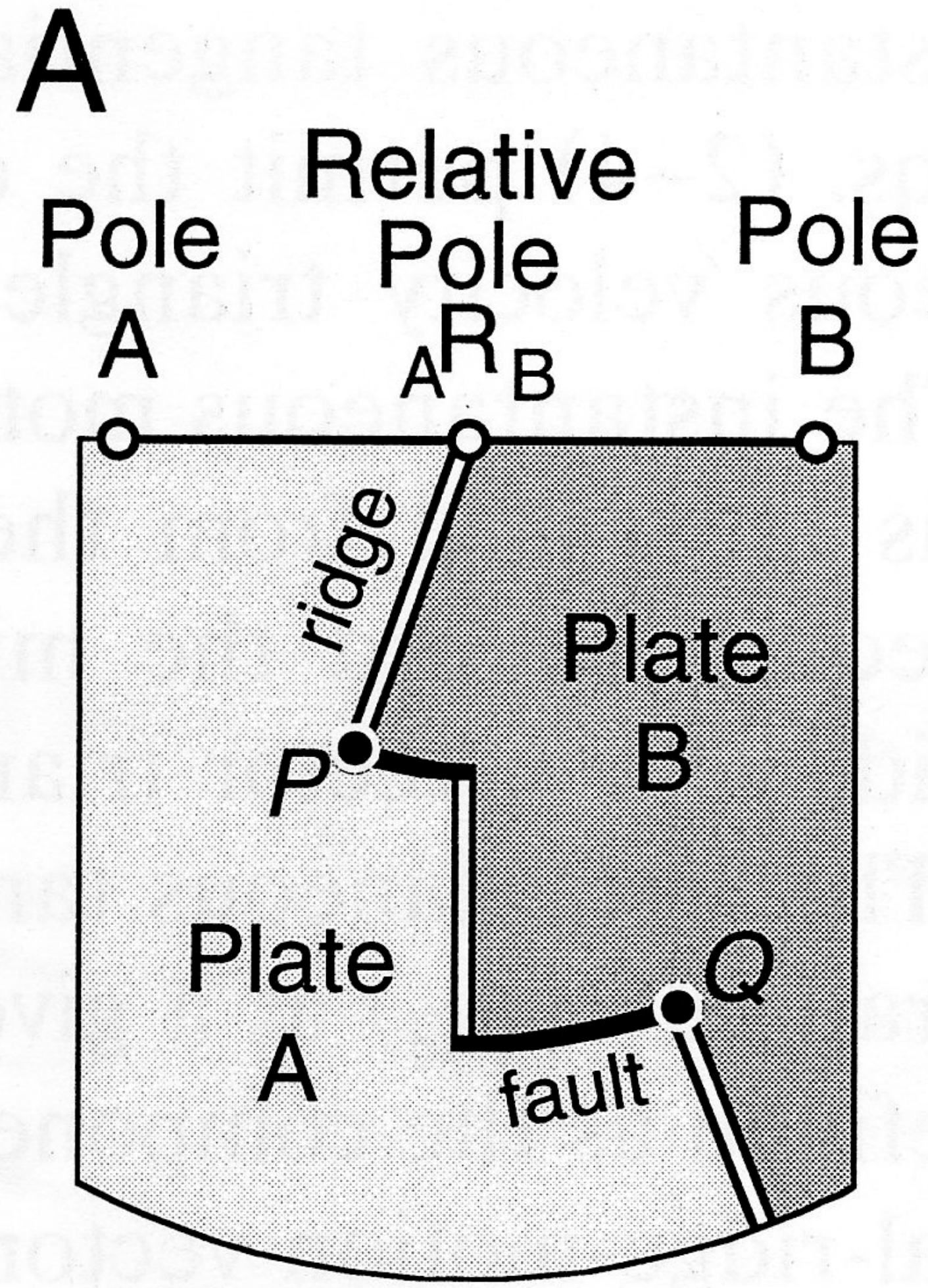
Vincent S. Cronin

Department of Geosciences, University of Wisconsin–Milwaukee, P.O. Box 413, Milwaukee, WI 53201, USA

(Received December 3, 1991; revised version accepted September 13, 1993)

Abstract

Intuition suggests that all points on the same mid-ocean ridge should rotate around the relative pole of the two-plate system at the same instantaneous angular velocity. Contrary to intuition, the instantaneous angular velocity of a ridge varies from one point to another along the ridge, given the general case in which two plates move around different plate-specific poles of rotation. The variation in the instantaneous angular velocity of a ridge is a function of the motion characteristics of the plates and the position of the ridge relative to the poles of plate motion. The length or orientation of individual ridge segments is predicted to vary over time, leading to local changes in the shape of the ridge. The gradient in instantaneous angular velocity for the fast-spreading East Pacific Ridge, between the Cocos and Pacific plates, is an order of magnitude greater than the gradient along the Mid-Atlantic Ridge, between the North American and African plates. This great contrast in ridge instantaneous velocity gradients may be reflected in the contrasting ridge geometries of the East Pacific and Mid-Atlantic Ridges.



$${}^1\boldsymbol{\omega}_2 = \boldsymbol{\omega}_2 - \boldsymbol{\omega}_1 \quad (1)$$

$$|\mathbf{v}_1| = |\boldsymbol{\omega}_1| \sin(r_{1Q}) \quad (2)$$

$$|\mathbf{v}_2| = |\boldsymbol{\omega}_2| \sin(r_{2Q}) \quad (3)$$

$$|{}^1\mathbf{v}_2| = |{}^1\boldsymbol{\omega}_2| \sin(r_{RP-Q}) \quad (4)$$

$$|\mathbf{v}_{\text{ridge}}| = \left(\frac{|{}^1\mathbf{v}_2|}{2} \right) - |\mathbf{v}_1| \cos(\theta_2) \quad (5)$$

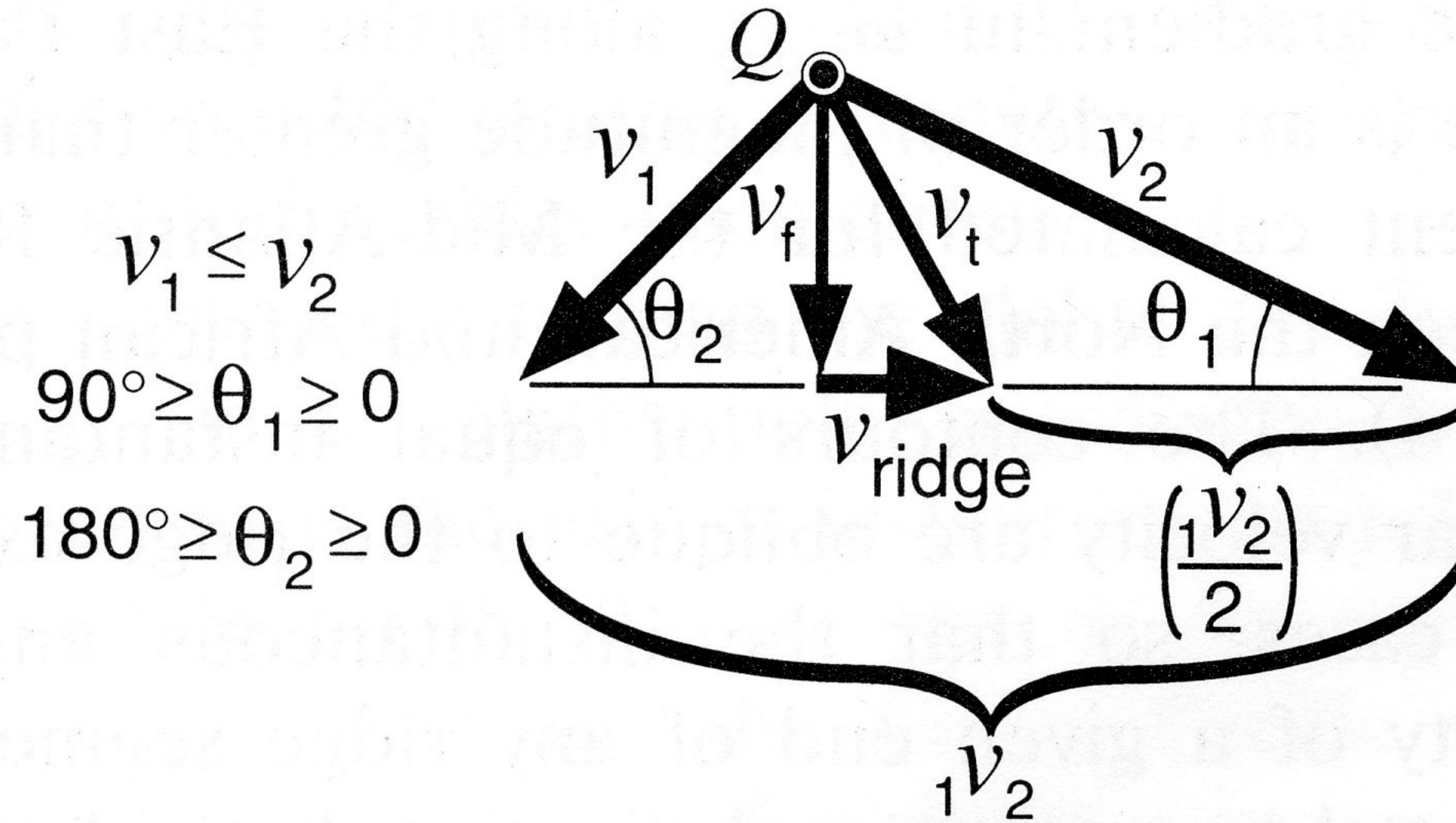
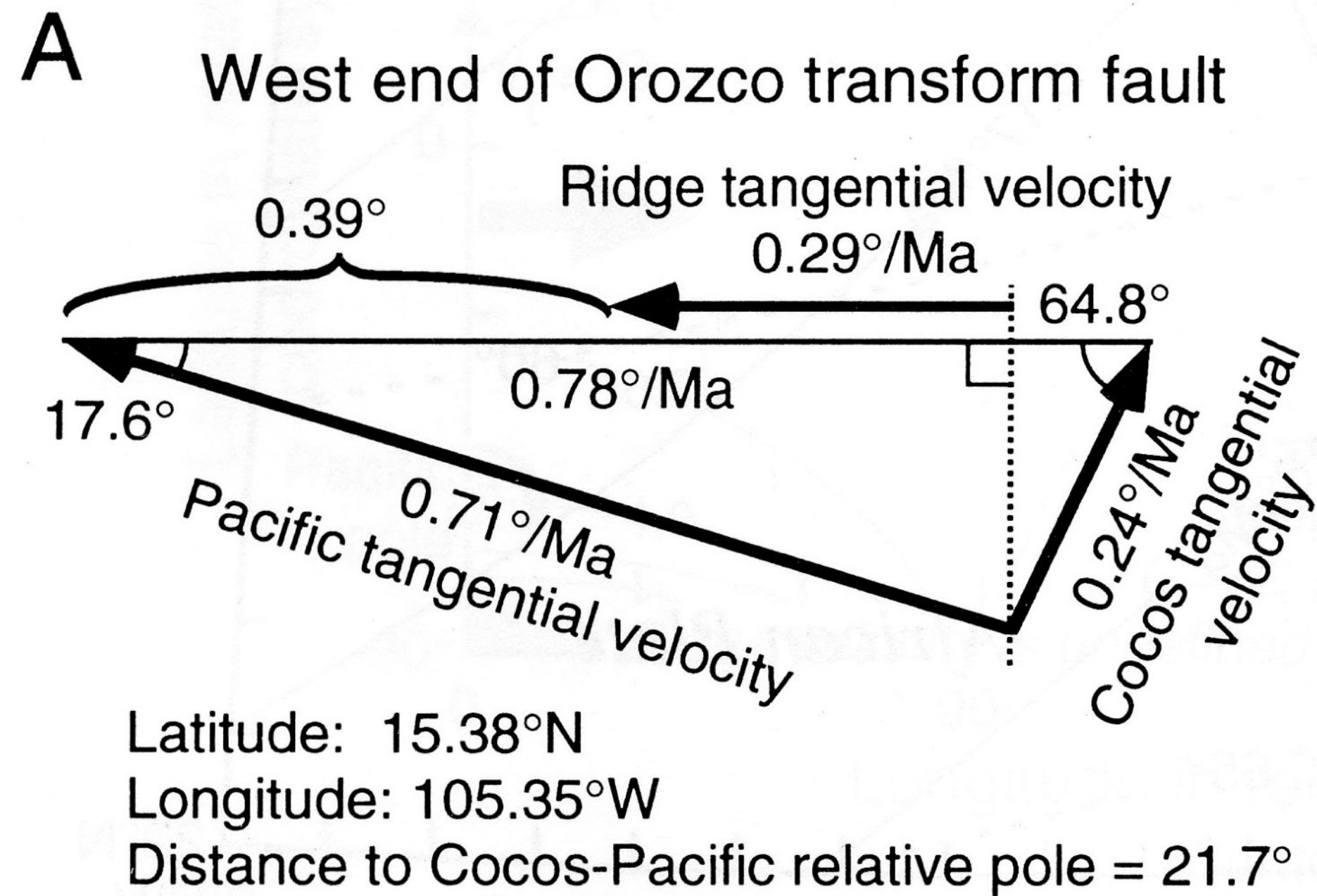
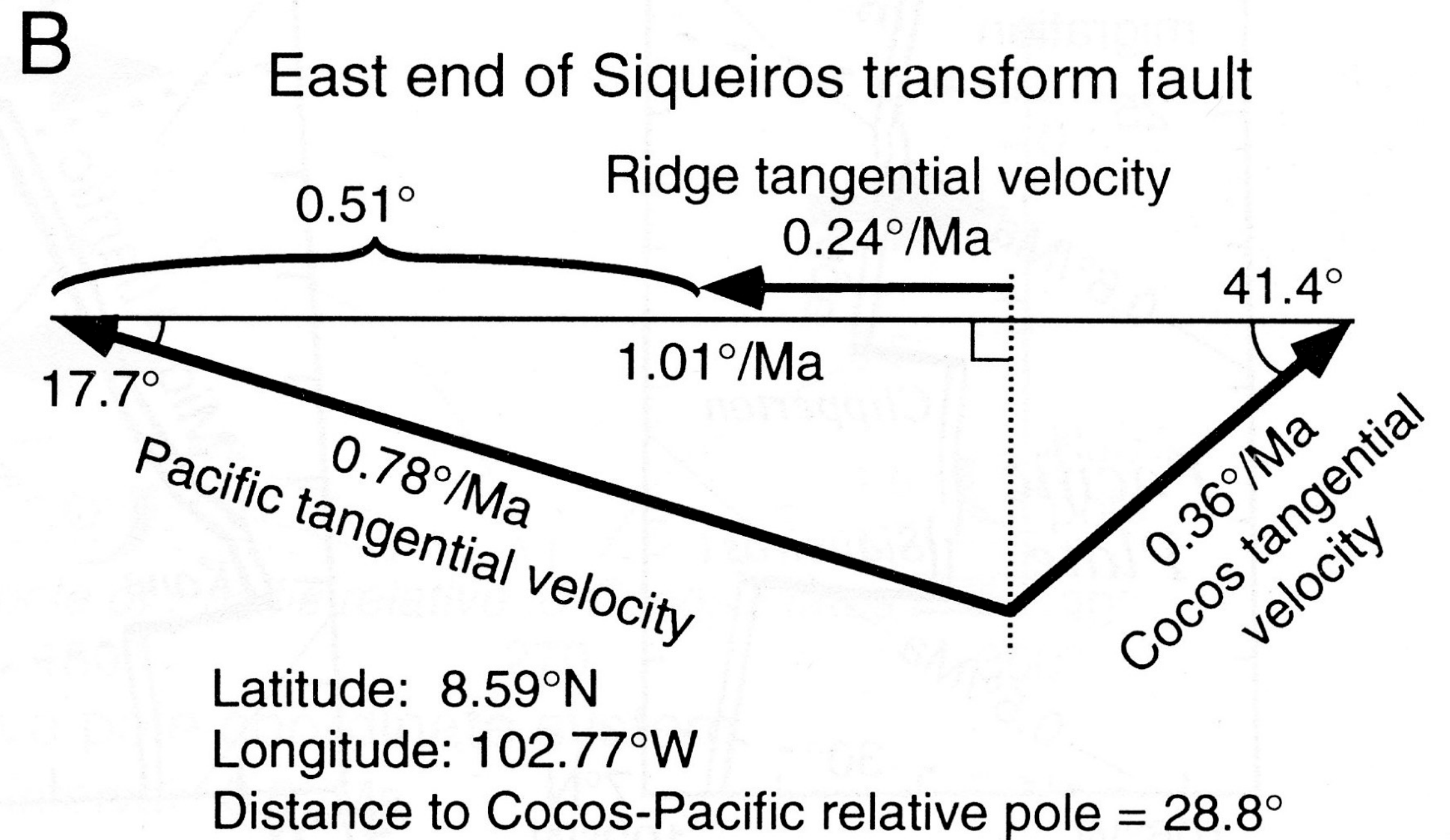


Fig. 2. Instantaneous tangential vector relationships at an arbitrary point along a ridge segment. Vectors v_1 and v_2 are the tangential velocities of the two plates resolved at the reference point, labeled so that magnitudes $|v_1| \leq |v_2|$. The ridge moves from the origin of v_1 and v_2 to the midpoint of $\frac{1}{2}v_2$ along total ridge motion vector v_t . Vector v_t has components v_f toward/away from the relative pole, and ridge migration vector v_{ridge} around the relative pole.

$$|\boldsymbol{\omega}_{\text{ridge}}| = \left(\frac{|\boldsymbol{v}_{\text{ridge}}|}{\sin(r_{\text{RP-Q}})} \right) \quad (6)$$

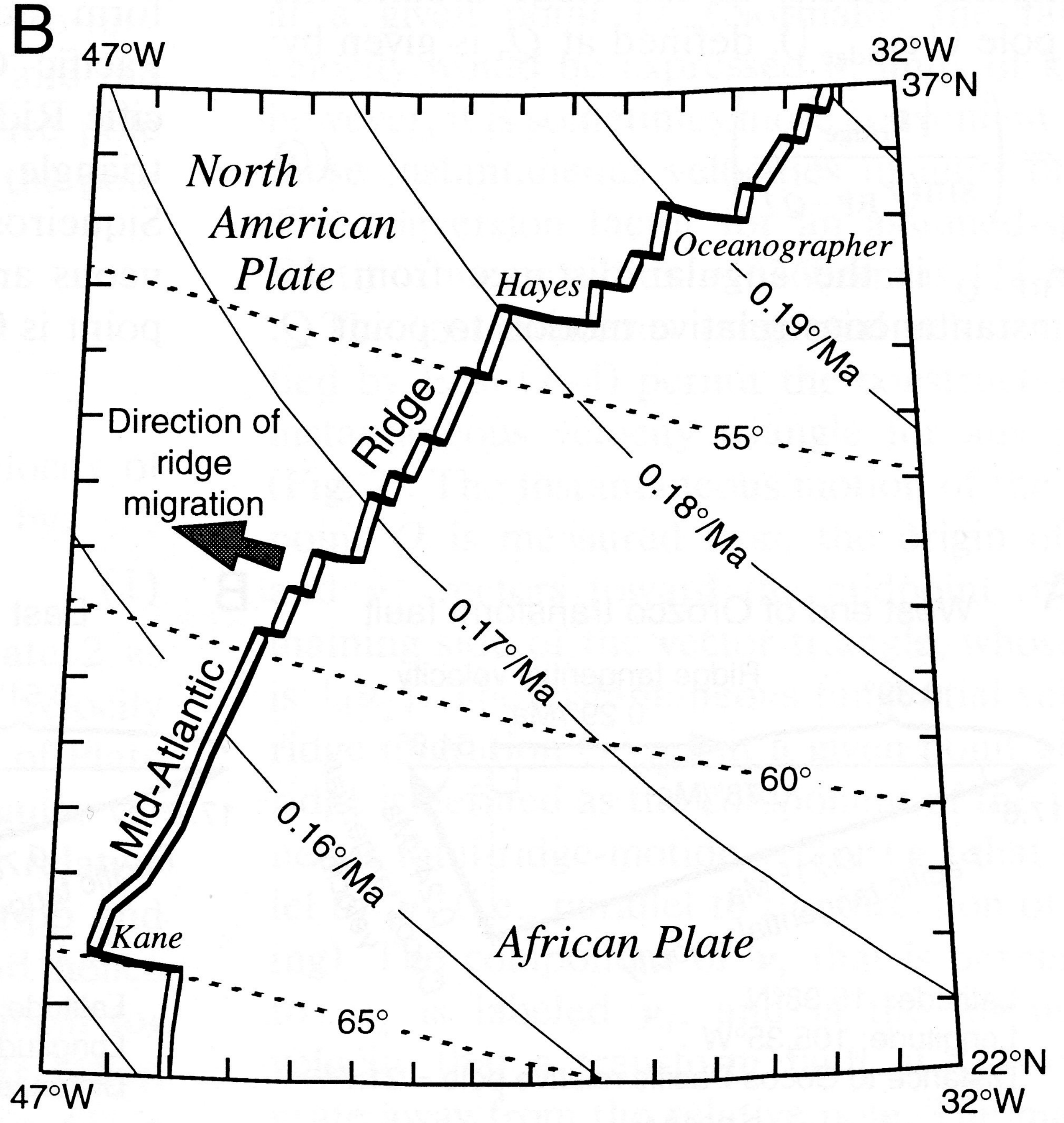
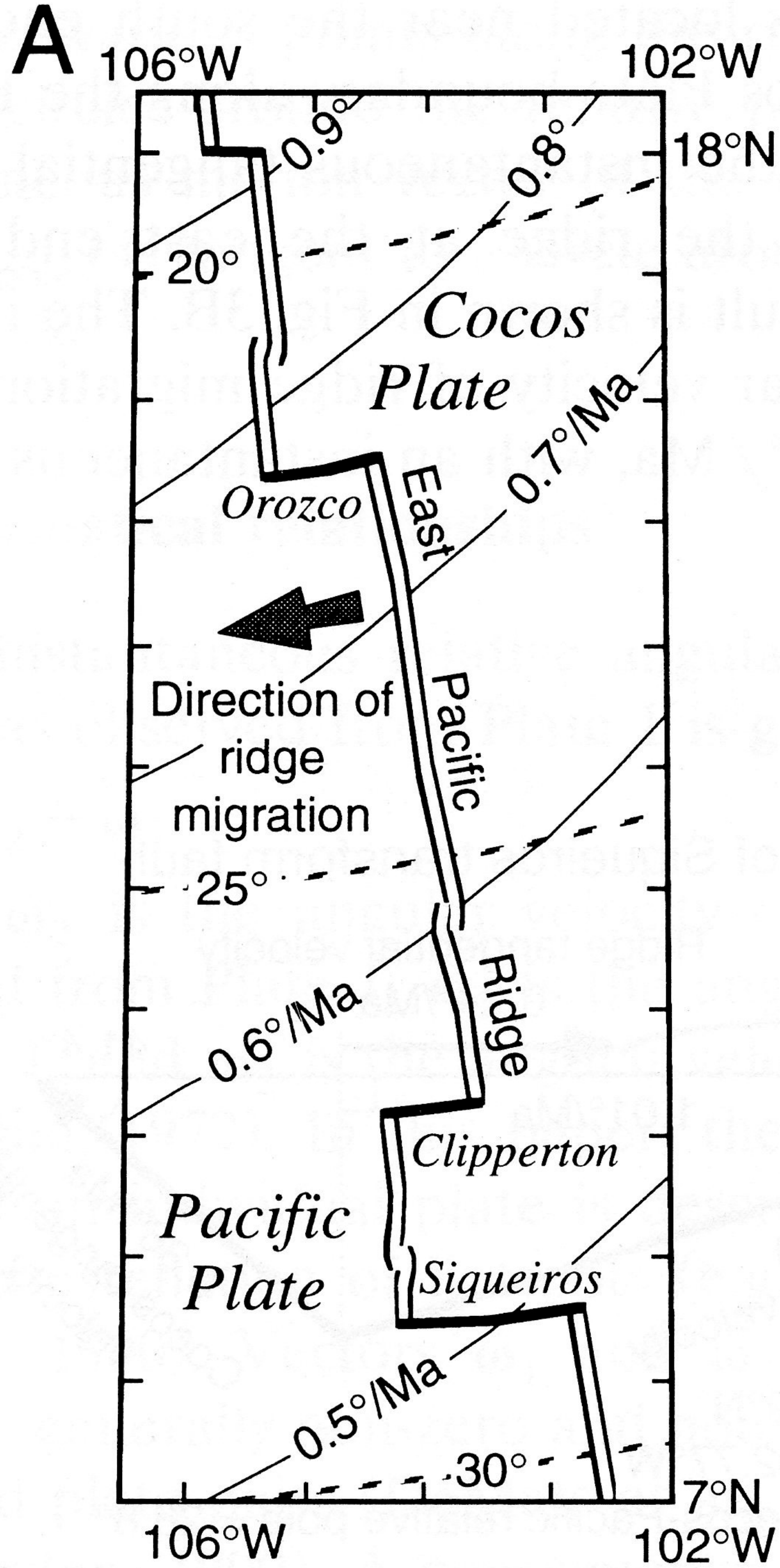


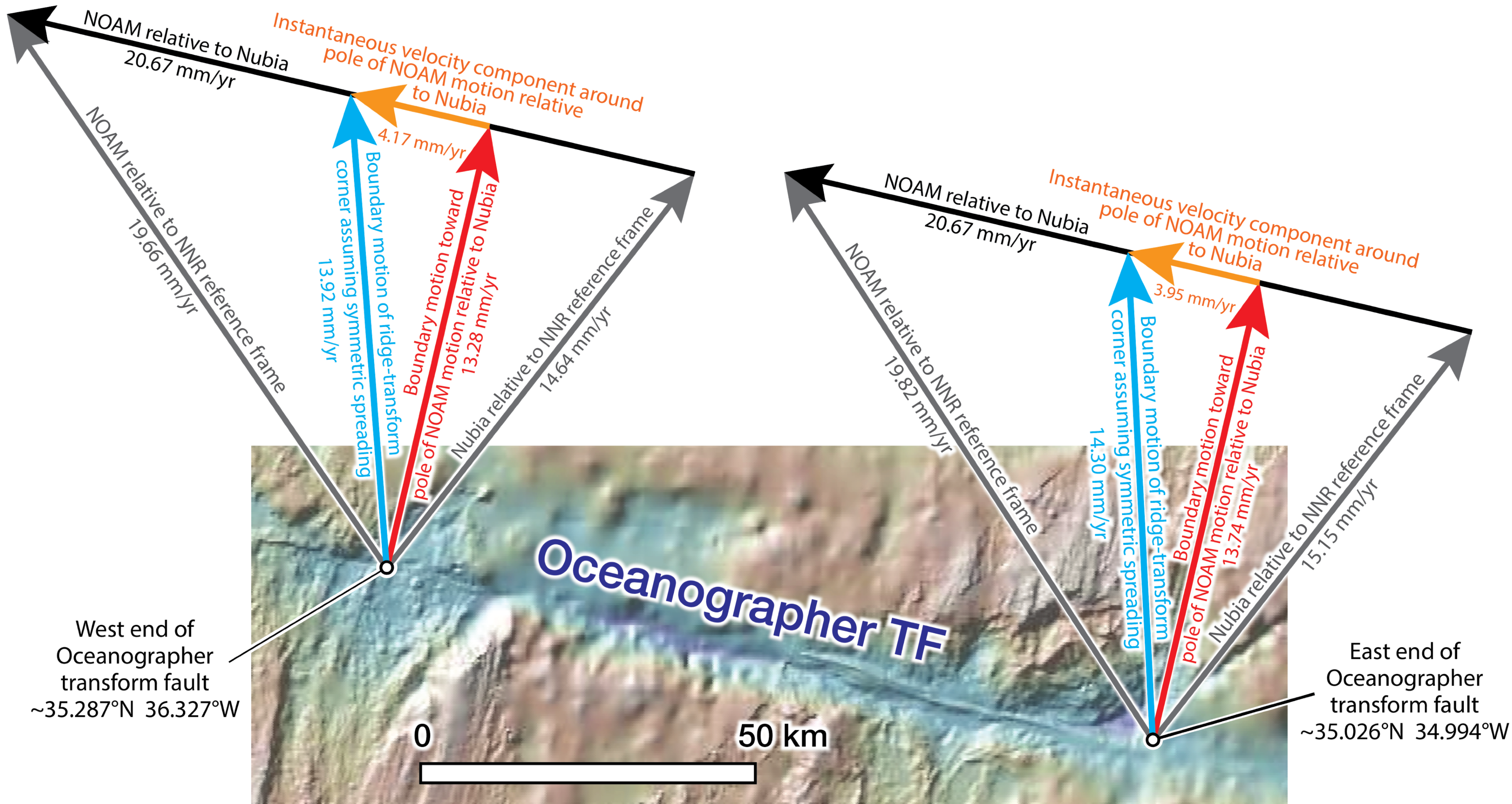
$$\omega_{\text{ridge}} = \frac{0.29^\circ/\text{Ma}}{\sin(21.7^\circ)} = 0.78^\circ/\text{Ma}$$

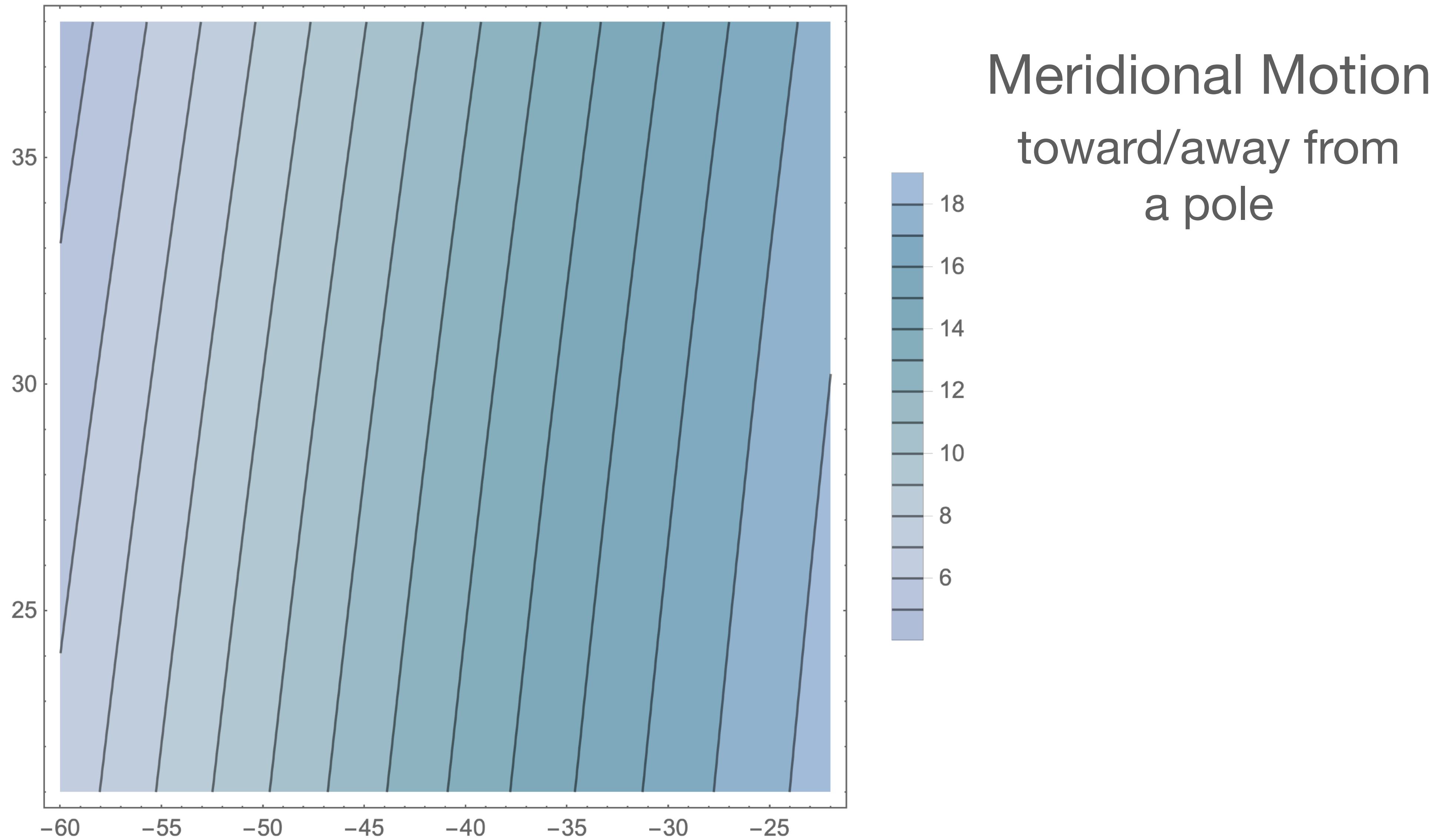


$$\omega_{\text{ridge}} = \frac{0.24^\circ/\text{Ma}}{\sin(28.8^\circ)} = 0.49^\circ/\text{Ma}$$

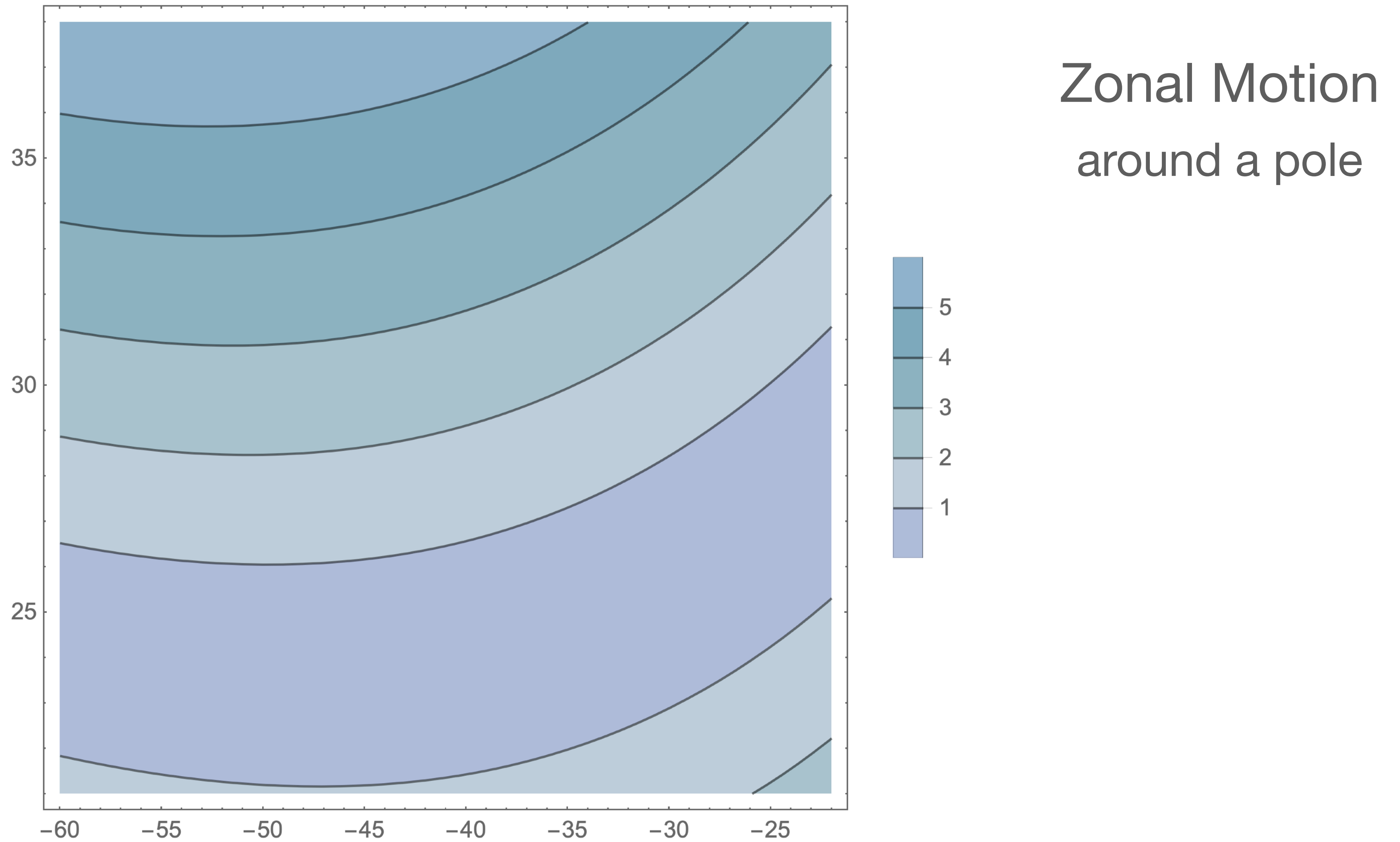
Fig. 3. Examples of instantaneous tangential velocity determinations for two points along the East Pacific Ridge between the Pacific and Cocos plates. (A) Vector relationships for the ridge terminus at the west end of the Orozco transform fault. (B) Vector relationships for the ridge terminus at the east end of the Siqueiros transform fault.



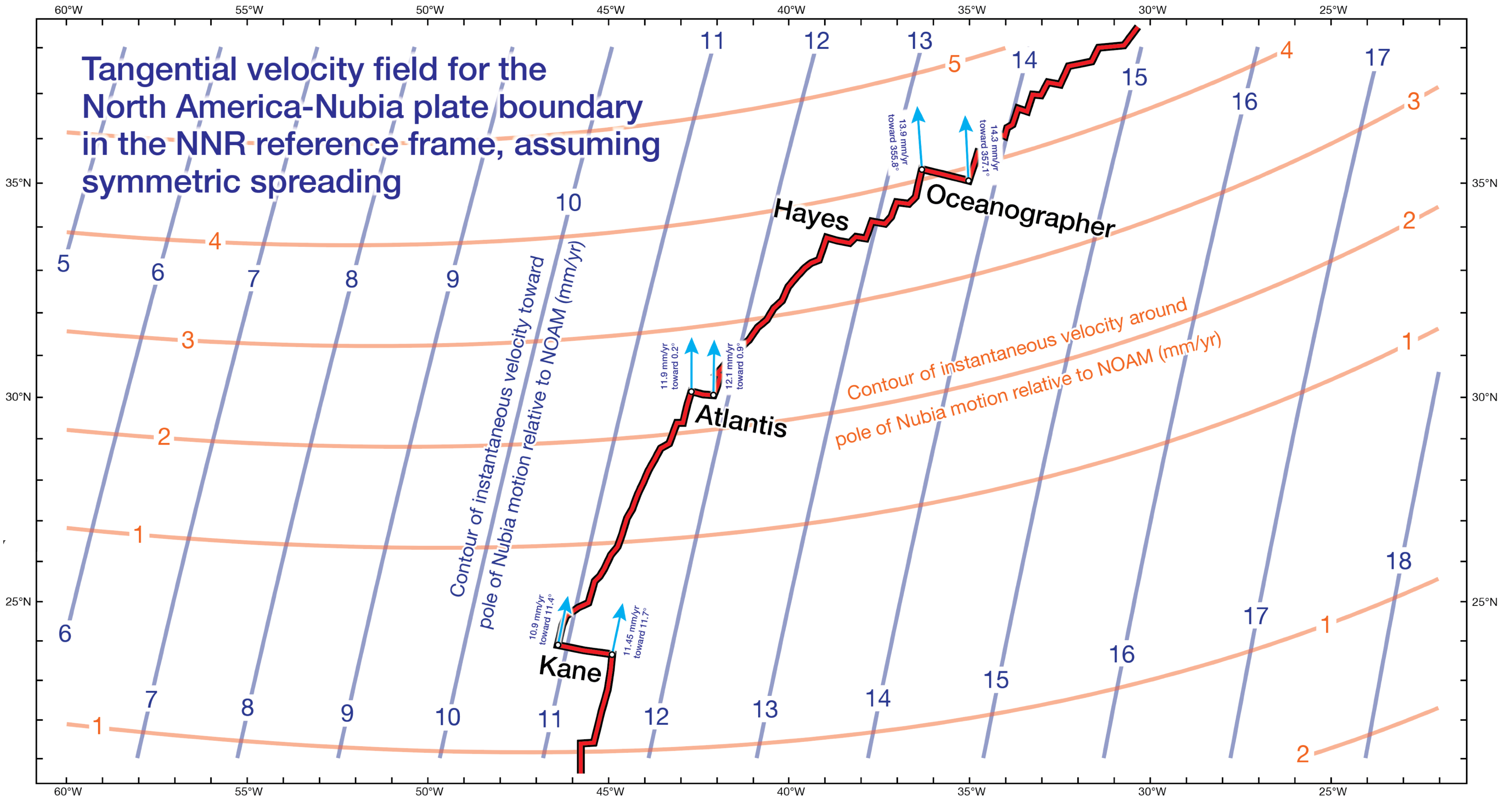




The map presented above shows instantaneous tangential speed contours reflecting the velocity field for points along a plate boundary moving toward/away from the poles of relative motion between the two plates.



The map presented above shows instantaneous tangential speed contours reflecting the velocity field for points along a plate boundary moving around the poles of relative motion between the two plates.



As the boundary moves in the NNR reference frame (Argus et al., 2011) over finite time intervals, the instantaneous velocity of each point along the boundary changes.

60°W 55°W 50°W 45°W 40°W 35°W 30°W 25°W

Location of selected isochron segments along the Kane, Atlantis and Oceanographer fracture zones

North American plate

Nubian plate

Hayes

Oceanographer

Atlantis

Kane

C13n-y

C6n-o

C5ADn-o

C3n.4n-o

C5n.2n-o

C6n-o

C13n-y

C13n-y

C6n-o

C5ADn-o

C3n.4n-o

C5n.2n-o

C6n-o

C13n-y

C22n-o

C13n-y

C6n-o

C5ADn-o

C3n.4n-o

C5n.2n-o

C6n-o

C13n-y

C22n-o

C13n-y

C6n-o

C5ADn-o

C3n.4n-o

C5n.2n-o

C6n-o

C13n-y

C13n-y

C6n-o

C5ADn-o

C3n.4n-o

C5n.2n-o

C6n-o

C13n-y

60°W 55°W 50°W 45°W 40°W 35°W 30°W 25°W

Base map from GeoMapApp